Catalysis Science & Technology

ROYAL SOCIETY OF CHEMISTRY

PAPER

View Article Online
View Journal | View Issue

Cite this: *Catal. Sci. Technol.*, 2021, **11**, 2403

Hydrogenation of dimethyl oxalate to ethylene glycol over Cu/KIT-6 catalysts†

Xinbin Yu,[a] Michael Burkholder,[b] Stavros G. Karakalos,[a] Gregory L. Tate,[a] John R. Monnier,[a] B. Frank Gupton[b] and Christopher T. Williams *[a]

Received 3rd December 2020,
Accepted 24th January 2021

DOI: 10.1039/d0cy02334e

rsc.li/catalysis

Copper supported on KIT-6 mesoporous silica was prepared *via* ammonia evaporation (AE) method and applied for the catalytic hydrogenation of dimethyl oxalate (DMO) to ethylene glycol (EG). The high specific surface area and interconnected mesoporous channels of the support facilitated the dispersion of copper species. The effect of AE temperature and copper loading on the structure of catalysts and induced change in hydrogenation performance were studied in detail. The results showed that both parameters influenced the overall and/or intrinsic activity. The hydrogenation of DMO to EG was proposed to proceed *via* the synergy between Cu^0 and Cu^+ sites and catalysts with high surface Cu^0/Cu^+ ratio exhibited high intrinsic activity in the investigated range.

1. Introduction

Ethylene glycol (EG) is a commodity widely consumed as a solvent, building block of polyester fibers, anti-freezing agent, alkyd resin and so forth.[1] Traditionally, EG is synthesized by hydration of ethylene oxide derived from petroleum feedstocks.[2] However, due to non-uniform global distribution of petroleum resources, the synthesis of EG from syngas is emerging as a rapidly growing technology, especially in Eastern Asia.[1,3] The process consists of producing syngas from coal, coupling of CO by methyl nitride on Pd/α-Al_2O_3 to form dimethyl oxalate (DMO), and subsequent hydrogenation of DMO to EG. This process has already been implemented on an industrial scale.[4]

The choice of catalysts is vital to the hydrogenation reaction, with CuCr catalysts having been found applicable to have excellent activity and stability.[5,6] However, the Cr^{6+} is a known health hazard and environmental pollutant, which motivates research for alternative, environmentally friendly catalysts. Along these lines, Cu/SiO_2 catalysts have proved effective for this reaction, due to the coexistence of surface Cu^0 and Cu^+ species that are proposed as sites for the activation of H_2 and C═O, respectively.[3,4] The Cu^0 species originate primarily from the reduction of CuO, while Cu^+ species come from the reduction of copper phyllosilicate ($Cu_2Si_2O_5(OH)_2$) and/or Cu–O–Si unit, which are the products of copper precursor species reacting with silica during the preparation of catalyst. Excellent performance of hydrogenation of DMO to EG can be achieved over Cu/SiO_2 by adjusting the balance of Cu^0 and Cu^+ sites.

Various promoters (B, Ni, Zn, La, Ag, Au, In, *etc.*) have been studied in detail to reveal how the surface content of Cu^0 and Cu^+ sites can be tuned for the optimal catalytic performance.[4,7–14] However, supports also play an important role as they not only help disperse the active species but also react with certain copper species to form copper phyllosilicate and/or Cu–O–Si unit. Ordered mesoporous silicas (*e.g.* MCM-41, SBA-15, and HMS) with tuneable mesopores, easily accessible internal surface, and high specific surface areas have been successfully applied as supports for metal catalysts in many reactions.[15,16] The spatial confinement exerted by channels on active species exhibits interesting phenomena, such as inhibiting particle growth and modifying product distribution. However, most of the studied mesoporous silicas for hydrogenation of DMO only have one- or two-dimensional pores.[11,12,17–19] These structures may suffer from problems such as inefficient utilization of active species due to blocked channels by particles (during preparation and reaction), coke and collapsed wall and inferior mass transfer kinetics.[18,19] Silicas with three dimensional, interconnected mesopores like KIT-6 would be a good choice to address these problems, and have not yet been explored as a support for the hydrogenation of DMO over Cu/SiO_2 catalysts.

Ammonia evaporation (AE) method is typically employed to deposit copper species onto silica supports like colloidal silica and mesoporous silicas since its invention by Ube

[a] *Department of Chemical Engineering, University of South Carolina, Columbia, SC 29208, USA. E-mail: willia84@cec.sc.edu*
[b] *Department of Chemical Engineering, Virginia Commonwealth University, Richmond, VA 23284-3068, USA*

† Electronic supplementary information (ESI) available. See DOI: 10.1039/d0cy02334e

Industries.[3,12] Many studies utilize this synthesis protocol to produce Cu/SiO_2 catalysts for DMO hydrogenation as it has been demonstrated to be more effective in dispersing copper species than wet impregnation.[12] As copper phyllosilicate and/or Cu–O–Si unit are generated by the reaction between copper–ammonia complexes and silica at the preparation stage, their content and the attendant change in the catalytic properties may be regulated by parameters such as ammonia evaporation temperature, pH, types of copper precursors, concentration of copper, calcination temperature, *etc.* Chen *et al.* found that ammonia evaporation temperature significantly influenced the deposited copper amount, relative content of Cu^+ and surface area of Cu^0 of reduced Cu/SiO_2 catalysts and the optimal temperature was 90 °C.[3] Yin *et al.* found that the surface ratio of Cu^0/Cu^+ could be adjusted by the copper loading, which then influenced both DMO hydrogenation activity and selectivity to EG.[20]

In the present work, ordered mesoporous silica with interconnected channels, KIT-6, is facilely synthesized by soft-templating method and then employed as support for copper catalysts prepared by ammonia evaporation method. The effect of AE temperature and copper loading on the performance and intrinsic activity of catalysts has been studied in detail. The catalysts are extensively characterized to investigate how the changes in surface properties (*i.e.* specific surface area of Cu^0 and surface ratio of Cu^0/Cu^+) induced by AE temperature and copper loading influence the catalytic performance.

2. Experimental

2.1. Materials

All the reagents in this work were commercially available. Copper(II) nitrate trihydrate (99%, Acros Organics), Pluronic® P-123 (average M_n ~5800, Sigma-Aldrich), HCl (37%, Sigma-Aldrich), dimethyl oxalate (99%, Sigma-Aldrich), tetraethyl orthosilicate (TEOS, 99.9%, Alfa Aesar), concentrated nitric acid (68–70%, BDH), *n*-butanol (99.5%, ACROS), ammonia aqueous solution (28%, BDH) were used without further purification. H_2 (UHP), He (UHP), Ar (UHP), N_2 (UHP), and air (zero grade) were purchased from Airgas. Deionized water (18 MΩ) was supplied by using a Milli-Q water system with Barnant B-pure filter.

2.2. Catalyst preparation

KIT-6 silica was prepared according to the reported method.[21,22] 13.5 g of Pluronic® P123 was mixed with 487.5 g of DI water and 26.1 g of HCl (37%) in a flask submerged in a silicone oil bath at room temperature. The mixture was vigorously stirred for 1 h and the temperature was increased to 35 °C. 13.5 g of *n*-butanol was added into the flask followed by stirring for another 1 h at 35 °C. Subsequently, 29 g of TEOS was added quickly into the solution and the mixture was stirred for 24 h at 35 °C. Then the temperature was elevated to 95 °C and maintained for 24 h (hydrothermal treatment). Afterward, the solid was filtrated and washed with adequate amount of DI water to remove Cl^- (tested with 0.1 M of $AgNO_3$ solution). The obtained white powder was dried for 12 h at 110 °C and then calcined in a furnace for 6 h at 550 °C.

Cu/KIT-6 catalysts were prepared by the ammonia evaporation (AE) method. For example, to prepare 10 wt% Cu/KIT-6, 3.8 g of $Cu(NO_3)_2{\cdot}3H_2O$ was dissolved in 100 ml of DI water. Then the pH of the solution was adjusted to 11 with certain amount of $NH_3{\cdot}H_2O$ (28%) and stirred for 1 h. 9 g of KIT-6 was added, and the suspension was stirred overnight. The pH of mixture was adjusted to 11 and then the mixture was heated in a silicone oil bath at 70 °C to remove NH_3. The evaporation process was terminated when the pH was less than 7. The mixture was then filtrated, washed three times with deionized water and dried overnight at 110 °C in an oven. Finally, the light blue powder was calcined in air at 400 °C for 3 h. The obtained calcined sample was denoted as 10Cu-70, where 10 was the weight percent loading of Cu on KIT-6 and 70 was the AE temperature. Samples with various copper loading (5 wt% and 20 wt%) and different AE temperature (80 °C, 90 °C and 100 °C) were prepared by the same method.

2.3. Catalyst characterization

N_2 physisorption at −196 °C was conducted to obtain information about the specific surface area and pore size on a Micromeritics ASAP 2020 instrument. Samples were heated at 120 °C for 2 h under vacuum prior to nitrogen adsorption. The calculation of specific surface area (S_{BET}) followed the Brunauer–Emmett–Teller (BET) method. Pore size distribution was evaluated by the Barrett–Joyner–Halenda (BJH) method using the data of desorption isotherm branch.

The composition of catalysts was measured by inductively coupled plasma-optical emission spectroscopy (ICP-OES, Perkin Elmer Avio 200). The surface area of metallic copper per gram of catalyst (S_{Cu^0}) was analyzed by N_2O titration method at 60 °C, assuming 1.46×10^{19} copper atoms per m^2. The formation amount (mole) of N_2 (equal to the consumption amount (mole) of N_2O by metallic Cu) was measured by a thermal conductivity detector (TCD).

The Fourier-transform infrared (FT-IR) spectra of calcined samples were obtained on Perkin Elmer Spectrum 100 FT-IR spectrometer at room temperature (4 scans for each spectrum). Diamond was used as an internal reflection element (IRE).

The reducibility of catalysts was analyzed on a Micromeritics Autochem II 2920 instrument to obtain the H_2 temperature-programmed reduction (H_2-TPR) profile. In a typical run, 100 mg of a calcined sample was reduced with 10% H_2/Ar (40 mL min^{-1}) with temperature ramping from RT to 600 °C at 5 °C min^{-1}. The consumption of H_2 was monitored by TCD.

The small angle X-ray scattering pattern of KIT-6 was collected on a SAXSLab Ganesha instrument. The sample was

scanned from 0.18 to 4 degree at a speed of 0.2 degree per minute at room temperature. Prior to the test, the instrument was calibrated with 640c silicon powder with the peak position fixed at the total scattering angle (2θ) of 28.44° according to the criteria of National Institute of Standards and Technology (NIST).

Wide-angle powder X-ray diffraction (XRD) patterns of catalysts were obtained on a Rigaku SmartLab SE X-ray diffractometer using Cu Kα radiation (λ = 0.15418 nm). For calcined samples, the XRD patterns were collected with a scanning angle (2θ) range from 10° to 90° at 15° min^{-1}. Prior to the measurement of reduced samples, calcined samples were *in situ* reduced with 10% H_2–90% N_2 mixture (100 mL min^{-1}) in a XRD reactor at 350 °C for 2 h. Then sample's XRD pattern at 350 °C and 190 °C was recorded with a scanning angle (2θ) range from 10° to 90° at 5° min^{-1}. The particle size was measured in terms of Scherrer equation using Cu(111) diffraction peak.

Transmission electron microscopy (TEM) was performed on a Hitachi HT7800 transmission electron microscope with an acceleration voltage of 100 kV. The samples were treated with procedures in our previous work to obtain finely dispersed suspension.[14] The suspension was then loaded onto a copper grid coated carbon film (300 mesh) and methanol completely evaporated at room temperature before loading the grid into the instrument.

X-ray photoelectron spectroscopy (XPS) was measured on a Kratos AXIS Ultra DLD XPS system with the same attachments and operation parameters in our previous work.[14] Calcined samples were *in situ* reduced at 350 °C for 2 h in a high temperature cell. Then XPS analysis was conducted when the samples reached room temperature. C1s binding energy (BE) of 284.8 eV was used as a reference to correct all the spectra.

2.4. Catalytic tests

Vapor-phase, catalytic hydrogenation of DMO was evaluated in a stainless-steel flow reactor. Typically, 0.6 g of calcined samples (40–60 mesh) was loaded into the reactor with internal diameter of 9.4 mm, sandwiched with adequate amount of quartz powder (20–40 and 40–60 meshes). Prior to the reaction, the calcined sample was reduced in 20% H_2–80% N_2 stream (75 mL min^{-1}) at 350 °C and atmospheric pressure for 4 h. The ramping rate was 2 °C min^{-1}. A 10 wt% DMO solution (in methanol) was introduced into the reactor by an ISCO pump (Teledyne ISCO) when the reactor cooled to the 190 °C and the system pressure reached 2.5 Mpa with the aid of a back-pressure regulator. The H_2/DMO molar ratio was kept 95 for all the runs. The condensed products were collected when the reaction was steady and analyzed on an Agilent 5890 Series II gas chromatograph with a flame ionization detector (FID) and RTX-Wax capillary column (30 m × 0.25 mm × 0.25 μm). The conversion of DMO and analysis of products (selectivity to methyl glycolate and ethylene glycol) were calculated in terms of the formulas below:

$$X_{DMO} = \frac{n_{DMO,in} - n_{DMO,out}}{n_{DMO,in}} \times 100$$

$$S_{MG} = \frac{n_{MG}}{n_{DMO,in} - n_{DMO,out}} \times 100$$

$$S_{EG} = \frac{n_{EG}}{n_{DMO,in} - n_{DMO,out}} \times 100$$

Other products included 1,2-butanediol (1,2-BDO), ethanol (EtOH) and 1,2-propanediol (1,2-PDO) and their selectivity was negligible. The standard deviation was calculated by the following formula:

$$S = \sqrt{\frac{1}{N-1} \times \sum_{i=1}^{N} (x_i - \bar{x})^2}$$

Measurements of turnover frequency (TOF, mol_{DMO}/($mol_{Cu\ on\ the\ surface}$ × h) or h^{-1}) were performed when the conversion of DMO was below 30% at the reaction condition (T, $P(H_2)$ and H_2/DMO molar ratio) listed above. The TOF value was calculated in terms of the specific surface area of Cu^0 measured by N_2O titration. It should be noted that the methanol produced from the reaction cannot be quantified due to the existence of a large excess of methanol (90 wt%) as solvent, as is standard for this reaction on both the lab scale and in industry.[3,12]

3. Results and discussion

3.1. Catalytic performance

The hydrogenation of DMO over KIT-6 supported copper catalysts was investigated in a flow reactor. The reaction proceeds *via* DMO to MG and then MG to EG, with further dehydration of EG producing other by-products like ethanol (Scheme 1). Fig. 1(A) shows the effect of AE temperature on the hydrogenation performance at 190 °C at the given conditions. All the 10 wt% Cu/KIT-6 prepared at different AE temperatures (70, 80, 90, 100 °C) showed roughly the same conversion of DMO (70–78%). The 10 wt% Cu/KIT-6 prepared at 90 °C showed slightly higher selectivity to EG and lower selectivity to MG. Thus, the AE temperature only slightly influence the hydrogenation performance, which is different from the significant effect of AE temperature on Cu/SiO_2 with colloidal silica as support in the hydrogenation of DMO to EG.[3] However, Fig. 1(B) and S2† show that the loading amount of copper species has a dramatic effect on the hydrogenation performance in terms of conversion of DMO and selectivity to EG, which is consistent with other reports.[18–20] Increasing the loading amount of Cu from 5 wt% to 20 wt% significantly improves the conversion of DMO and selectivity to EG. The performance of 5 wt% Cu/KIT-6 is tested at 195 °C because it shows very low activity at 190 °C. The positive correlation between activity and loading amount

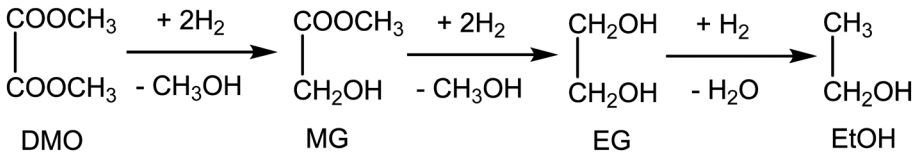

Scheme 1 Simplified reaction pathways for the hydrogenation of DMO to MG, EG, and ethanol.

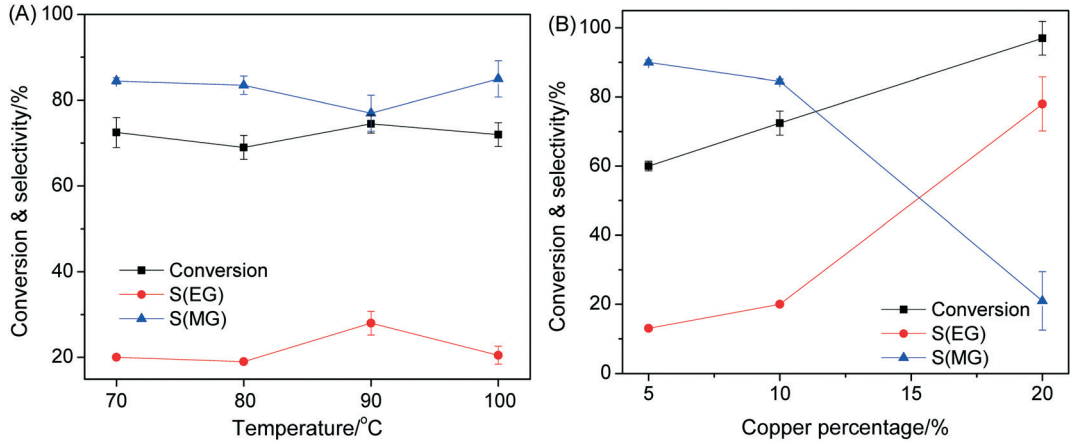

Fig. 1 (A). Effect of temperature of evaporating NH_3 on hydrogenation of DMO over 10 wt% Cu/KIT-6, (B). Effect of copper weight percentage on hydrogenation of DMO over Cu-70, reaction condition: T = 190 °C and 195 °C for 5Cu-70, $P(H_2)$ = 2.5 MPa, H_2/DMO molar ratio = 95, WHSV = 0.66 h^{-1}.

of Cu is explained by the increase in the amount of active sites and/or the formation of more intrinsically active sites when elevating Cu loading amount over KIT-6, which will be discussed in the following section.

Fig. 2 shows the stability of hydrogenation of DMO over 20 wt% Cu/KIT-6 prepared at 70 °C. The catalyst does not show any deactivation after 221 h on stream. The fluctuations in the selectivity are an artifact of the small uncertainties in the GC measurements that are amplified in the calculation of denominator in the selectivity equations above.

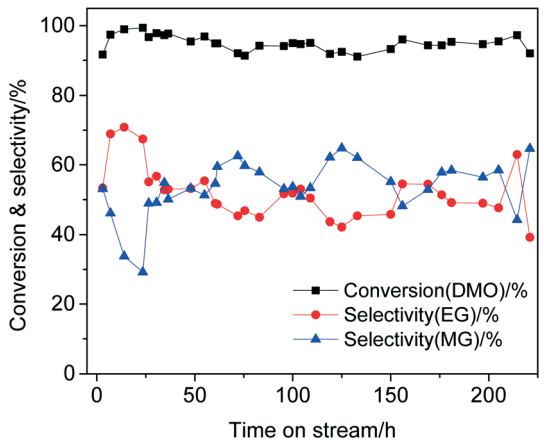

Fig. 2 Stability test of hydrogenation of DMO over 20 wt% Cu/KIT-6 prepared at 70 °C, reaction condition: T = 190 °C, $P(H_2)$ = 2.5 MPa, H_2/DMO molar ratio = 95, WHSV = 0.66 h^{-1}.

3.2. Material characterizations

Several characterizations have been performed to gain an insight into the effect of AE temperature and loading amount of Cu on the structure of Cu/KIT-6 catalysts. Fig. 3 shows the structural characterizations of bare KIT-6. The pattern (Fig. 3(A)) exhibits peaks at 0.92° (211), 1.01° (220) and 1.75° (420), indicating that the support has cubic *Ia3d* symmetry with interconnected channels.[22] The TEM image (Fig. 3(B)), N_2 adsorption–desorption isotherm pattern (Fig. 3(C)) and BJH pore size distribution analysis (Fig. 3(D)) confirm that the support has mesopore structure with mesopore diameter of 6.6 nm. Moreover, a certain amount of pores in the micropore/small mesopore range is observed, which is attributed to the secondary pore system in the framework walls (*i.e.*, intra-wall pores) providing interconnections for adjacent mesopores (Fig. 3D).[23–27]

The bulk properties and compositions of representative catalysts are summarized in Table 1. ICP-OES confirms that the real deposited amount of copper species on KIT-6 *via* ammonia evaporation method is close to the target weight percentage in the investigated range. All the calcined samples exhibit type IV isotherms revealed by N_2 physisorption (Fig. 4). The pore diameter distribution plot shows that all the samples have mesopores with pore diameter of ~6 nm with certain amount of pores in the micropore/small mesopore range, similar to mesopore diameter of bare support. The bare KIT-6 support has a specific surface area of 703 m^2 g^{-1}. The specific surface area decreases to

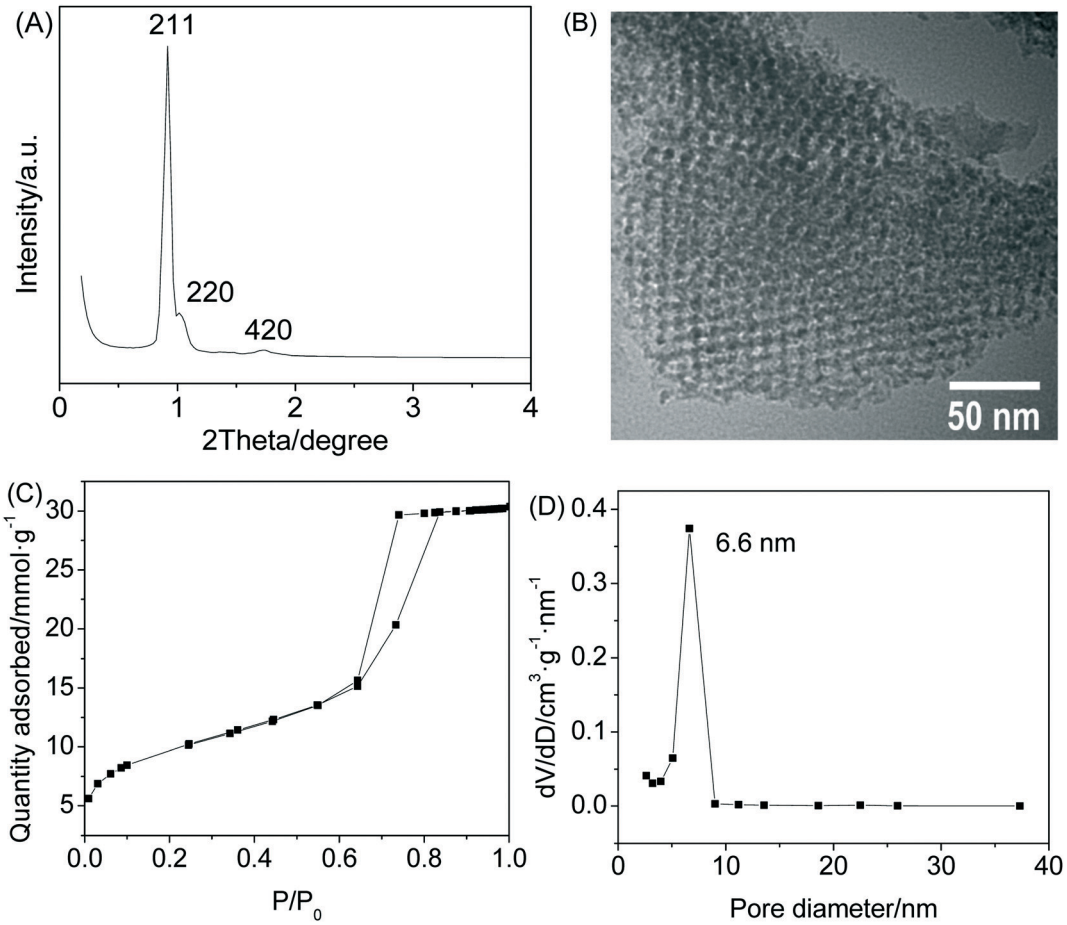

Fig. 3 Structural characterizations of KIT-6, (A). SAXS pattern (B). TEM image, (C). N_2 adsorption–desorption isotherm, (D). BJH pore size distribution.

Table 1 Physicochemical and catalytic properties of Cu/KIT-6 catalysts

Sample	Cu content,[a] /wt%	S_{BET},[b] /m^2 g^{-1}	V_p,[c] /cm^3 g^{-1}	S_{Cu},[d] /m^2 g^{-1}	d_p,[e] /nm	TOF,[f] /h^{-1}
KIT-6	0	703	1.03	~	~	~
5Cu-70	5.7	305	0.90	~	2.1	~
10Cu-70	10.4	294	0.84	2.81	2.8	63.3 ± 4.5
10Cu-80	10.3	294	0.84	2.93	~	49.9 ± 6.9
10Cu-90	11.3	290	0.85	2.84	~	87.8 ± 0.5
10Cu-100	10.5	280	0.85	2.47	~	58.5 ± 6.5
20Cu-70	19.7	268	0.69	4.55	3.2	99.4 ± 10.4

[a] Determined by ICP-OES analysis. [b] BET specific surface area. [c] Pore volume at $P/P_0 = 0.99$. [d] Surface area of Cu^0 per gram of catalyst measured by N_2O titration method. [e] Average crystallite size measured in terms of Cu(1 1 1) peak at 190 °C. [f] TOF value calculated in terms of specific surface area of Cu^0 from N_2O titration results.

305 m^2 g^{-1} upon the loading of 5 wt% of copper species. However, the specific surface area does not change significantly for samples with 10 wt% and 20 wt% of copper species. Besides, only small change (~10%) in pore volume exists when comparing 5Cu-70 sample with bare support. Based on these observations, we think that copper species are deposited on the external surface, in intra-wall pores and mesopores and more mesopore volume is occupied when the deposited amount of copper is higher (*e.g.* 20 wt%). Similar analysis has been reported by other researchers.[20,25]

Fig. 5 shows the FT-IR spectra of calcined KIT-6 and Cu-containing samples to gain an insight into the existing copper species on the calcined samples. It is observed that copper could form copper phyllosilicate and/or Cu–O–Si unit with silica at the preparation stage. The absence of the peak at 670 cm^{-1} attributed to the δ_{OH} band of copper phyllosilicate indicates that copper phyllosilicate may not exist on the Cu-containing samples.[18,20] The peaks located at 800 cm^{-1} and 1061 cm^{-1} are assigned to the symmetric and asymmetric ν_{SiO} band of amorphous silica, respectively. The

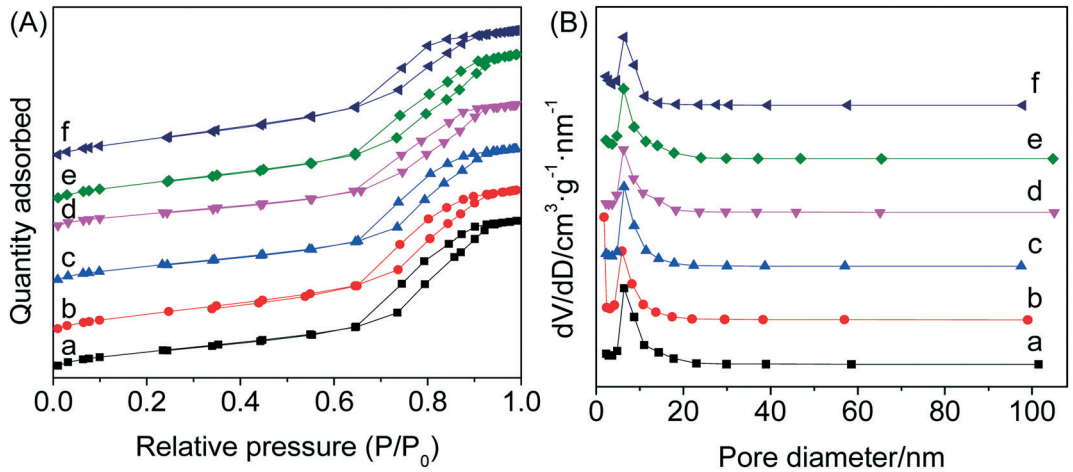

Fig. 4 (A) N_2 adsorption–desorption isotherms and (B) BJH pore size distribution of the calcined catalysts of different copper loadings. a. 5Cu-70, b. 10Cu-70, c. 10Cu-80, d. 10Cu-90, e. 10Cu-100, f. 20Cu-70.

peaks at 1643 cm^{-1} are ascribed to the bending mode of OH groups of adsorbed water. No peaks at 690 cm^{-1} belonging to the bending absorption of the Cu–OH bond exist confirming the absence of copper hydroxide on the calcined samples. The peak at 970 cm^{-1} is assigned to the Si–O stretching of Si–OH structure, with both the intensity and band width influenced by the formation of Cu–O–Si, where the Si–O is still present, but with the H is replaced by Cu.[18] The ratio of peak intensities at 970 cm^{-1} and 800 cm^{-1} (I_{970}/I_{800}) is therefore calculated to estimate the amount of incorporated copper as the peak at 800 cm^{-1} represents the symmetric ν_{SiO} band of KIT-6 and the change in the intensity of peak at 970 cm^{-1} originates from incorporated copper.[18] The gradual increase in I_{970}/I_{800} when elevating the loading amount of copper as listed in Fig. 5 suggests that a certain amount of copper is incorporated into the framework of KIT-6. No copper hydroxide or copper phyllosilicates exist over the calcined Cu/KIT-6 samples, unlike Cu/SiO_2 prepared with colloidal silica as silica source.[7,9,14]

Fig. 6 shows the H_2-TPR profiles of different catalysts to reveal their reducibility. All the profiles exhibit a single peak centered at different temperature, attributed to the collective reduction of Cu^{2+} and Cu^{+} species (see XPS section) to Cu^0 and/or Cu^{+}. The reduction temperature (185–206 °C) in our case is significantly lower than the typical reduction temperature of Cu/SiO_2 catalysts (243–270 °C) reported in literature, implying that copper species are well dispersed on KIT-6.[3,17–19,28] This is correlated well with TEM and XRD measurements. Comparing the peak positions reveals that the peak gradually shifts to higher temperature when increasing the loading amount of Cu. It has been reported that supported CuO with smaller crystallites is much more facile to be reduced than bulk CuO.[3,29] *In situ* XRD results reveal that elevating the loading amount of Cu causes an increase in average size of crystallites. Thus, the shift is attributed to increasing copper particle sizes and decrease in the dispersion.

The existing copper species on the calcined samples can be a mixture of Cu^{+} species, CuO with different dispersions

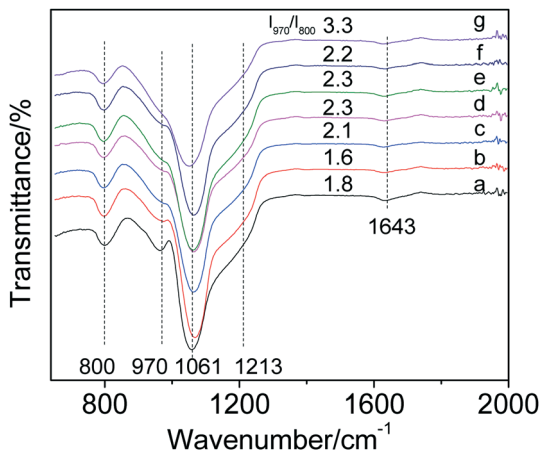

Fig. 5 FT-IR spectra of different calcined samples, a. KIT-6, b. 5Cu-70, c. 10Cu-70, d. 10Cu-80, e. 10Cu-90, f. 10Cu-100, g. 20Cu-70.

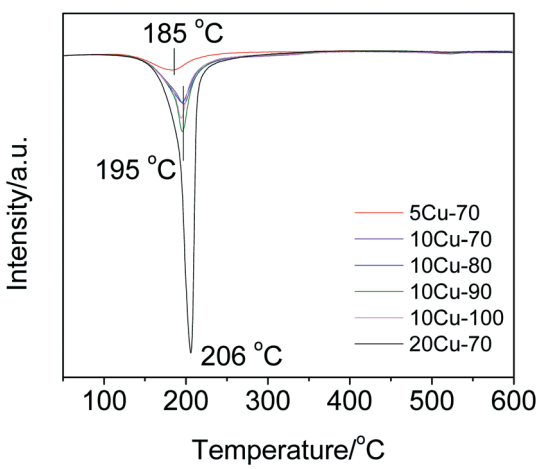

Fig. 6 H_2-TPR profiles of different catalysts.

and Cu–O–Si structures, although the profile only shows one reduction peak for every sample. Van der Grift *et al.* and Marchi *et al.* found that the reduction of the copper phyllosilicate and ion-exchanged Cu–O–Si species to Cu^+ could overlap with the reduction of well dispersed CuO to Cu^0.[30,31] FT-IR spectra show that Cu–O–Si structure rather than copper phyllosilicate is present on the Cu-containing samples, in accordance with others reports with ordered mesoporous silica as support.[18,20] H_2-TPR might not differentiate different copper species present on the calcined samples due to their difference in the amount and reducibility. XPS results show that both Cu^0 and Cu^+ species exist on the surface of samples reduced at 350 °C, which suggests that not only one type of copper species exist on the calcined samples. Further reduction of Cu^+ species originating from Cu–O–Si structure may require a much higher temperature to destroy their stable structures.[30,31]

Wide-angle powder XRD patterns of the calcined and reduced samples were obtained to differentiate the existing phases and calculate crystallite sizes. No noticeable peaks assigned to metal oxides exhibit on calcined samples (Fig. 7(A)) implying that copper species are highly dispersed on the support. Two peaks (Fig. 7(B)) at 43.5° and 74.4° attributed to Cu^0(111) and Cu^0(220) emerge after *in situ* reduction at 350 °C.[14,18,32,33] The small peak at around 50° on the reduced samples may be attributed to the Cu(200) peak, although it is partially obscured by the background feature.[12,33] The peaks become more intense and sharper as the loading amount of copper species increase, implying the growth in particle size. The average particle sizes are calculated according to Scherrer equation (Table 1). It shows the average particle sizes grow with the increase in the loading amount of copper as it becomes more difficult to disperse metal oxides well on the support when elevating their loading amount.[34,35] The average particle sizes are all around 3 nm, confirming that the copper species are highly dispersed on the catalysts. The Cu particles sizes in our case are also smaller than Cu particles supported over other ordered mesoporous silicas.[18,20,28]

Fig. 8 shows the TEM images of representative Cu/KIT-6 catalysts. All the catalysts maintain the characteristics of the mesoporous structure, and the copper species are clearly well-dispersed along the channels, substantiating the analysis in H_2-TPR and XRD sections. Furthermore, the uniform distribution of copper species along the channels suggests that the high specific surface area and interconnected mesoporous channels of the support may facilitate the Cu dispersion compared with similar catalysts employing ordered mesoporous silicas as support.[18–20] The copper species distributed on KIT-6 are not in the form of typical spherical particles which makes us unable to calculate the average particle sizes from TEM images.

The specific surface area of Cu^0 was measured by N_2O titration method as listed in Table 1. The specific surface area of Cu^0 for all the samples with 10 wt% Cu is roughly the same and it increases significantly when elevating the loading amount of copper species.

XPS measurements with X-ray induced Auger electron spectroscopy (XAES) were conducted to reveal chemical states of copper species and their relative content on calcined samples and reduced catalysts. For Cu 2p XPS spectra of calcined samples (Fig. 9(A)), the peak at around 934.7 eV is assigned to Cu^{2+} species, confirmed by the characteristic satellite peak at 943.0 eV.[3,7,14] The peak at around 932.8 eV is attributed to Cu^+ species. The Cu^+ might be generated by thermally removing oxygen atom from CuO lattice during the calcination stage as Cu_2O species are more thermodynamically stable than CuO species at high temperature. Only reduced copper species are present on the surface after reduction, evidenced by the existence of two peaks at 932.8 eV and 953.0 eV (Fig. 9(B)), assigned to Cu 2p3/2 and Cu 2p1/2 of reduced copper species, respectively.[3,7,14] Consistent with these assignments, the satellite peaks with Cu 2p binding energy of 943.0 eV assigned

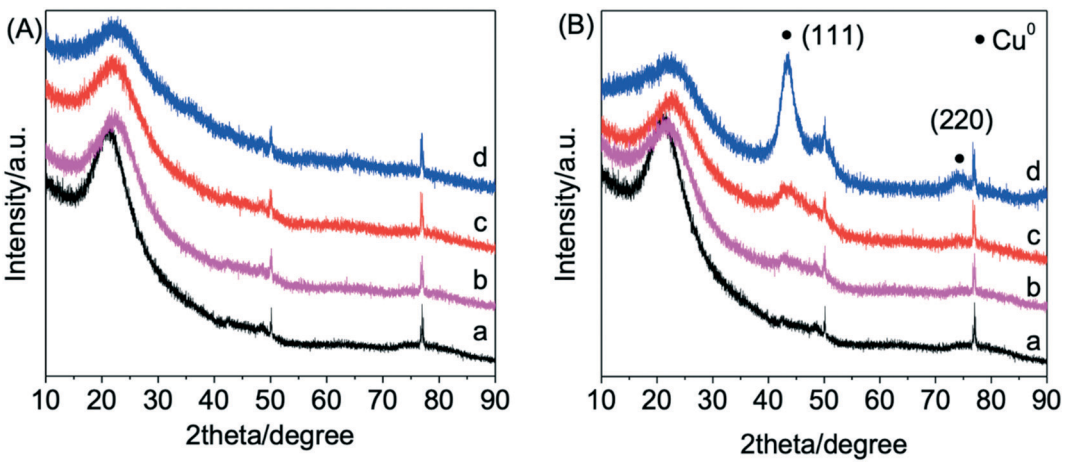

Fig. 7 (A). XRD patterns of calcined samples at room temperature, (B) *In situ* XRD patterns of reduced catalysts at 190 °C, a. a blank XRD reactor, b. 5Cu-70, c. 10Cu-70, d. 20Cu-70.

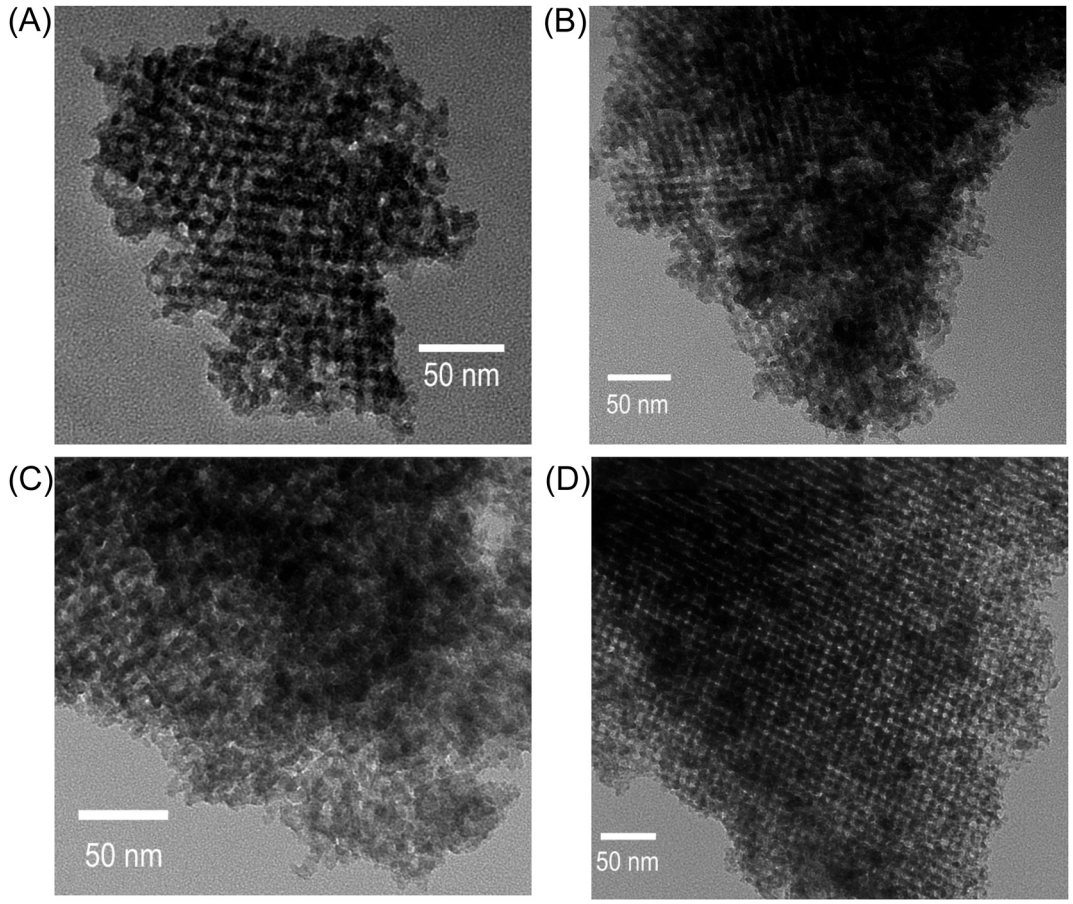

Fig. 8 TEM images of (A) 5Cu-70, (B) 10Cu-70, (C) 20Cu-70, (D) 20Cu-70 after stability test.

to Cu^{2+} species are absent. The XPS results confirm that surface Cu^{2+} species are reduced to Cu^0 and/or Cu^+ species.

Cu LMM XAES spectra were obtained to further distinguish the chemical states of copper species (Cu^0 and Cu^+) present on the reduced surface by the difference in their kinetic energies. The co-existence of Cu^0 and Cu^+ species on reduced samples is proved by two visible peaks with Auger kinetic energy of 913.5 eV and 917.5 eV (Fig. 9(C)).[3,7,14] Peak deconvolution is employed to calculate the relative content of near-surface Cu^0 and Cu^+ species. The results (Table 2) show that the surface content of Cu^+ species for samples prepared at 70 °C (5 wt%, 10 wt% and 20 wt%) decreases with the increasing loading amount of Cu. This might be explained by the increased difficulty to disperse copper species at higher loadings. Interestingly, 10 wt% Cu/KIT-6 prepared at 90 °C shows lower Cu^+ content than other 10 wt% Cu/KIT-6 samples prepared at 70 °C, 80 °C, 100 °C, which might be attributed to the effect of temperature on the growth of different copper species.

3.3. Discussion

The optimization of Cu/SiO_2 catalysts for the hydrogenation of DMO to EG has been intensively studied in terms of promoters for copper species and morphologies of supports. With respect to the support, it not only disperses active species, but also can react with a certain amount of copper species to generate the precursor of Cu^+ species. In addition, effective supports should help inhibit the growth of copper particles, since the Hüttig temperature of copper is low and sintering is actually the most significant problem for Cu/SiO_2 catalysts. Thus, ordered mesoporous silicas with high specific surface area and well-defined pore structure have been utilized for the hydrogenation of DMO. Yin *et al.* prepared hexagonal mesoporous silica (HMS) support copper catalysts by an impregnation method.[28] They found that HMS supports with large pore diameters and specific surface areas facilitated the dispersion of the active copper species and exhibited large copper surface areas, which then improved the performance of DMO hydrogenation.[28] Ma *et al.* fabricated mesoporous MCM-41 supported copper catalysts for hydrogenation of DMO to EG, and attributed the excellent performance to the high dispersion of copper species and large specific surface areas of copper.[18] As high metal dispersion is one of the keys to enhance the hydrogenation activity of Cu/SiO_2 catalysts, ordered mesoporous silicas with high specific surface area and interconnected mesoporous channels would be an excellent choice because they may facilitate the homogenous deposition of copper species during the preparation stage. Characterizations (XRD, TEM

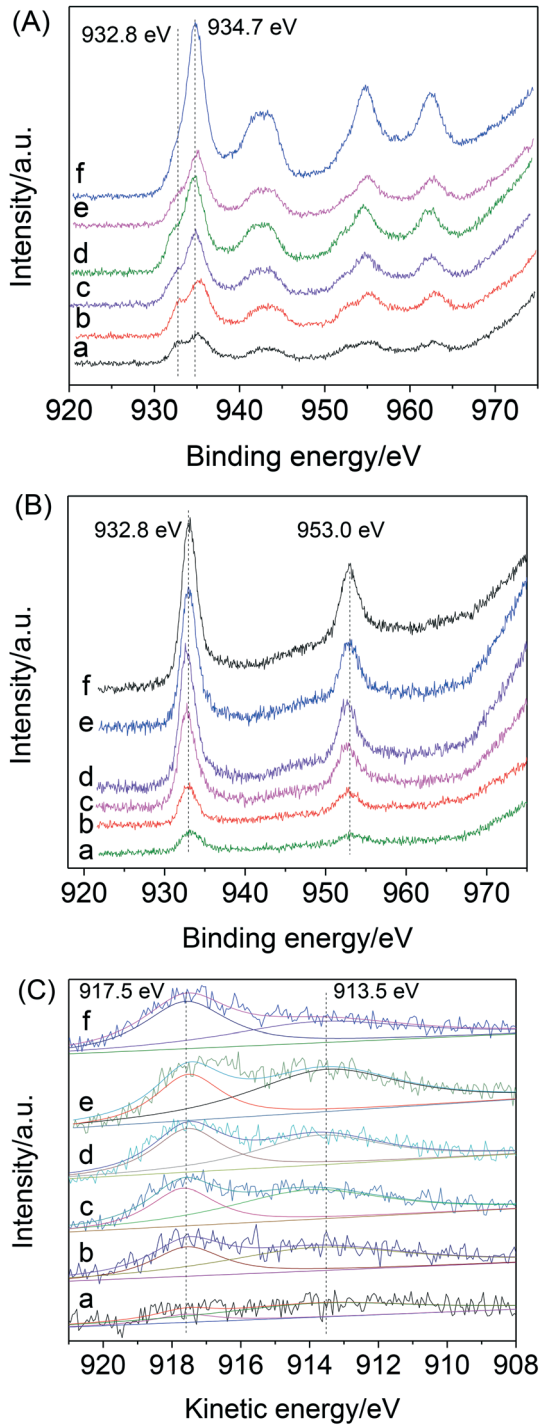

Fig. 9 (A) Cu 2p XPS spectra of calcined samples, (B) Cu 2p XPS spectra and (C) Cu LMM XAES spectra of reduced catalysts, a. 5Cu-70, b. 10Cu-70, c. 10Cu-80, d. 10Cu-90, e. 10Cu-100, f. 20Cu-70.

and H_2-TPR) confirm that the KIT-6 supported copper catalysts exhibit excellent dispersions of copper. TEM measurements shows that 20Cu-70 catalyst still maintains a good dispersion of copper species along the channels after 221 h stability test. Compared with other mesoporous silica (HMS and MCM-41) supported Cu catalysts, catalysts with KIT-6 as support could offer smaller metallic Cu particles at similar copper loading amount although the synthesized HMS and MCM-41 have much higher specific surface area.[18,28] It may indicate that the interconnected channels can facilitate the transfer of copper species during the preparation of catalysts.

As the AE method is widely used to prepare Cu/SiO_2 catalysts, it is worthwhile to consider the effect of various preparation parameters (*e.g.* loading amount of Cu and pH) on both the absolute amount and relative content of Cu^+ and Cu^0 species on the surface as well as the resulting change in the performance and intrinsic activity of the catalysts. However, most of the related research focuses on catalysts with support from colloidal silica. Yin *et al.* found that the initial precipitation temperature significantly influenced the textural properties of Cu/SiO_2 catalysts and surface content of copper species.[36] The observed enhancement in the catalytic performance was attributed to the high dispersion of copper species and suitable ratio of Cu^0/Cu^+. Zhao *et al.* studied hydrogenation of DMO over ordered mesoporous silica (OMS) supported copper catalysts.[19] They found that appropriate pH value of the mixture of $[Cu(NH_3)_4]^{2+}$ and OMS could preserve the mesoporous structure and proper loading amount of copper species could facilitate the dispersion of copper. The sample with high surface areas of Cu^0 and Cu^+, and the highest ratio of $Cu^+/(Cu^0 + Cu^+)$ showed the best performance. In the present case, the loading amount of copper species exhibits a more significant effect on the performance of Cu/KIT-6 in terms of conversion of DMO and selectivity to EG than AE temperature in the investigated range. It is explained by that more active sites will be available when increasing the loading amount of copper.

It is often proposed that hydrogenation of DMO to EG happens *via* a synergism between balanced amount of Cu^0 and Cu^+ species.[3,37–40] Poels *et al.* studied the hydrogenation of methyl acetate and suggested that Cu^0 species were sites for the activation of hydrogen molecules and the Cu^+ species were active sites for adsorption of the methoxy and acyl species.[38] In this case, the two distinct peaks of the Cu LMM XAES spectra confirm that both Cu^0 and Cu^+ species exist on the surface of all the reduced Cu/KIT-6 catalysts. For Cu/SiO_2 catalysts with colloidal silica as support, copper phyllosilicate is observed over the calcined samples which accounts for the Cu^+ species over the reduced catalysts. However, our study and the results from other groups indicate that copper phyllosilicate is not present over the calcined Cu/SiO_2 samples with ordered mesoporous silica as the support and the Cu^+ species over the reduced catalysts are proposed to originate from the reduction of Cu–O–Si unit.[18,20] The results suggest the types of silica influence the formation of copper phyllosilicate. As Cu^+ species are Lewis acid sites, Yin *et al.* proposed that the activation of C═O bond might be facilitated on Cu^+ species *via* the electron lone pair on oxygen atom in the hydrogenation of DMO to EG.[20] Although catalysts with balanced amount of Cu^0 and Cu^+ sites on the surface could exhibit excellent performance, it is still not clear what ratio of $Cu^+/(Cu^+ + Cu^0)$ is best for the catalysts and whether the surface should be Cu^0-rich or Cu^+-rich to

Table 2 Deconvolution results of XPS and Cu LMM XAES of reduced catalysts

Catalyst	KE,[a] eV		AP,[b] eV		Cu $2p_{3/2}$ BE, eV	X_{Cu^+},[c] %	Cu^0/Cu^{+d}
	Cu^+	Cu^0	Cu^+	Cu^0			
5Cu-70	913.7	917.6	1846.6	1850.5	932.9	86	0.16
10Cu-70	913.8	917.6	1846.7	1850.5	932.9	68	0.47
10Cu-80	914.0	917.7	1846.8	1850.5	932.8	65	0.54
10Cu-90	913.7	917.5	1846.4	1850.2	932.7	56	0.79
10Cu-100	913.7	917.7	1846.6	1850.6	932.9	68	0.47
20Cu-70	913.7	917.6	1846.6	1850.5	932.9	50	1.0

[a] Kinetic energy. [b] Auger parameter. [c] Ratio of peak areas between Cu^+ and (Cu^+ + Cu^0) by deconvolution of Cu LMM XAES spectra under the assumption that the Cu^+ ions and Cu^0 atoms occupy identical areas and have identical atomic sensitivity factors. [d] Cu^0/Cu^+ is calculated by $(1 - X_{Cu^+})/X_{Cu^+}$.

achieve high intrinsic activity. For Cu/SiO_2 catalysts with colloidal silica and some types of ordered mesoporous silica as support, the best performance is usually achieved on catalysts with the highest $Cu^+/(Cu^+ + Cu^0)$. However, Yin *et al.* found that Cu/HMS catalysts with the highest ratio of Cu^0/Cu^+ were most active for DMO hydrogenation and exhibited the highest selectivity to EG.[20] Zhao *et al.* suggested that surface area of Cu^0 species might be the key parameter for the DMO hydrogenation on Cu/OMS catalysts.[19] In our case, all the 10Cu/KIT-6 samples exhibit roughly the same Cu^0 surface area but the highest turnover frequency is achieved on 10Cu-90 with lowest surface Cu^+ content. It is substantiated by 20Cu-70 sample with high surface Cu^0/Cu^+ ratio which also shows very high intrinsic activity. Thus, surface Cu^0/Cu^+ ratio is decisive to the intrinsic activity of hydrogenation of DMO on Cu/KIT-6 catalysts. It is noted that the conversion of DMO over 10 wt% Cu/KIT-6 is almost independent on AE temperature. However, the turnover frequency over 10Cu-90 sample is much higher than the turnover frequency obtained over other 10 wt% Cu/KIT-6 samples. The explanations are as-following. First, it is uncertain that whether diffusion limitations are ruled out or not at the catalytic evaluation conditions (T = 190 °C, $P(H_2)$ = 2.5 MPa, H_2/DMO molar ratio = 95, WHSV = 0.66 h^{-1}). Second, the hydrogenation of MG to EG also happens over Cu^0 and Cu^+ sites and the selectivity to EG is higher over 10Cu-90 sample when comparing with other 10 wt% Cu/KIT-6 catalysts in the catalytic evaluation. Third, turnover frequency measures the activity per site, which is not the same as the results obtained in catalytic evaluation. Above all, the results suggest that high surface Cu^0/Cu^+ ratio is beneficial to the high intrinsic activity of Cu/KIT-6 catalysts in the hydrogenation of DMO to EG.

4. Conclusions

KIT-6 supported copper catalysts are prepared *via* ammonia evaporation (AE) method. The high specific surface area and inter-connected mesoporous channels of the support facilitate the dispersion of copper species along the channels. The particles still maintain a high dispersion even after nine days during the stability test. The effect of AE temperature and loading amount of copper are studied to optimize the performance of DMO hydrogenation on Cu/KIT-6 catalysts. AE temperature does not influence the hydrogenation performance achieved over 10 wt%/KIT-6 significantly, but it has a noticeable effect on the intrinsic activity. The loading amount of copper species influences both the hydrogenation performance and intrinsic activity. The effect of AE temperature and loading amount of copper species on intrinsic activity is attributed to induced change in the ratio of Cu^0/Cu^+ on the surface and high Cu^0/Cu^+ ratio on the surface favors the hydrogenation of dimethyl oxalate in this case.

Conflicts of interest

There are no conflicts to declare.

Acknowledgements

The project is sponsored by National Science Foundation of United States (#CBET-1510157) and National Science Foundation of United States – Industry/University Cooperative Research Center for Rational Catalyst Synthesis (#IIP-1464630). This work made use of the South Carolina SAXS Collaborative. The authors thank Eric Williams for the help on SAXS.

References

1 H. R. Yue, Y. J. Zhao, X. B. Ma and J. L. Gong, *Chem. Soc. Rev.*, 2012, **41**, 4218–4244.
2 P. P. McClellan, *Ind. Eng. Chem.*, 1950, **42**, 2402–2407.
3 L. F. Chen, P. J. Guo, M. H. Qiao, S. R. Yan, H. X. Li, W. Shen, H. L. Xu and K. N. Fan, *J. Catal.*, 2008, **257**, 172–180.
4 Z. He, H. Q. Lin, P. He and Y. Z. Yuan, *J. Catal.*, 2011, **277**, 54–63.
5 L. R. Zehner and R. W. Lenton, *US Pat.*, 4112245, 1978.
6 M. Haruhiko, H. Kouichi, U. Taizou, N. Yasuo, I. Seizou and T. Takanori, *JP Pat.*, 57123127, 1982.
7 A. Y. Yin, C. Wen, X. Y. Guo, W. L. Dai and K. N. Fan, *J. Catal.*, 2011, **280**, 77–88.
8 W. Qi, L. Qiu, D. Ding, Y. Z. Chen, C. W. Shi, P. Cui, Y. Wang, Q. H. Zhang, R. Liu and H. Shen, *Catal. Commun.*, 2018, **108**, 68–72.
9 X. L. Zheng, H. Q. Lin, J. W. Zheng, X. P. Duan and Y. Z. Yuan, *ACS Catal.*, 2013, **3**, 2738–2749.

10 Y. Huang, H. Ariga, X. L. Zheng, X. P. Duan, S. Takakusagi, K. Asakura and Y. Z. Yuan, *J. Catal.*, 2013, **307**, 74–83.
11 J. W. Zheng, H. Q. Lin, Y. N. Wang, X. L. Zheng, X. P. Duan and Y. Z. Yuan, *J. Catal.*, 2013, **297**, 110–118.
12 A. Y. Yin, J. W. Qu, X. Y. Guo, W. L. Dai and K. N. Fan, *Appl. Catal., A*, 2011, **400**, 39–47.
13 Y. N. Wang, X. P. Duan, J. W. Zheng, H. Q. Lin, Y. Z. Yuan, H. Ariga, S. Takakusagi and K. Asakura, *Catal. Sci. Technol.*, 2012, **2**, 1637–1639.
14 X. B. Yu, T. A. Vest, N. Gleason-Boure, S. G. Karakalos, G. L. Tate, M. Burkholder, J. R. Monnier and C. T. Williams, *J. Catal.*, 2019, **380**, 289–296.
15 H. J. Chae, T. W. Kim, Y. K. Moon, H. K. Kim, K. E. Jeong, C. U. Kim and S. Y. Jeong, *Appl. Catal., B*, 2014, **150**, 596–604.
16 J. Liang, Z. Liang, R. Zou and Y. Zhao, *Adv. Mater.*, 2017, **29**, 1701139.
17 X. Y. Guo, A. Y. Yin, W. L. Dai and K. N. Fan, *Catal. Lett.*, 2009, **132**, 22–27.
18 X. B. Ma, H. W. Chi, H. R. Yue, Y. J. Zhao, Y. Xu, J. Lv, S. P. Wang and J. L. Gong, *AIChE J.*, 2013, **59**, 2530–2539.
19 Y. J. Zhao, Y. Q. Zhang, Y. Wang, J. Zhang, Y. Xu, S. P. Wang and X. B. Ma, *Appl. Catal., A*, 2017, **539**, 59–69.
20 A. Y. Yin, X. Y. Guo, W. L. Dai and K. N. Fan, *J. Phys. Chem. C*, 2009, **113**, 11003–11013.
21 S. Schünemann, G. Dodekatos and H. Tüysüz, *Chem. Mater.*, 2015, **27**, 7743–7750.
22 F. Kleitz, S. H. Choi and R. Ryoo, *Chem. Commun.*, 2003, 2136–2137.
23 K. Soni, B. S. Rana, A. K. Sinha, A. Bhaumik, M. Nandi, M. Kumar and G. M. Dhar, *Appl. Catal., B*, 2009, **90**, 55–63.
24 B. Zhou, C. Y. Li, N. Qi, M. Jiang, B. Wang and Z. Q. Chen, *Appl. Surf. Sci.*, 2018, **450**, 31–37.
25 C. M. A. Parlett, A. Aydin, L. J. Durndella, L. Frattini, M. A. Isaacs, A. F. Lee, X. T. Liu, L. Olivi, R. Trofimovaite, K. Wilson and C. F. Wu, *Catal. Commun.*, 2017, **91**, 76–79.
26 R. Guillet-Nicolas, R. Ahmad, K. A. Cychosz, F. Kleitz and M. Thommes, *New J. Chem.*, 2016, **40**, 4351–4360.
27 R. Kishor and A. K. Ghosha, *Microporous Mesoporous Mater.*, 2017, **242**, 127–135.
28 A. Y. Yin, X. Y. Guo, W. L. Dai, H. X. Li and K. N. Fan, *Appl. Catal., A*, 2008, **349**, 91–99.
29 Z. Liu, M. D. Amiridis and Y. Chen, *J. Phys. Chem. B*, 2005, **109**, 1251–1255.
30 C. J. G. Van Der Grift, A. Mulder and J. W. Geus, *Appl. Catal.*, 1990, **60**, 181–192.
31 A. J. Marchi, J. L. G. Fierro, J. Santamaría and A. Monzon, *Appl. Catal., A*, 1996, **142**, 375–386.
32 S. Zhao, H. R. Yue, Y. J. Zhao, B. Wang, Y. C. Geng, J. Lv, S. P. Wang, J. L. Gong and X. B. Ma, *J. Catal.*, 2013, **297**, 142–150.
33 J. Ding, T. Popa, J. K. Tang, K. A. M. Gasem, M. H. Fan and Q. Zhong, *Appl. Catal., B*, 2017, **209**, 530–542.
34 J. X. Chen, Y. Yang, H. Shi, M. F. Li, Y. Chu, Z. Y. Pan and X. B. Yu, *Fuel*, 2014, **129**, 1–10.
35 X. B. Yu, J. X. Chen and T. Y. Ren, *RSC Adv.*, 2014, **87**, 46427–46436.
36 A. Y. Yin, X. Y. Guo, W. L. Dai and K. N. Fan, *Catal. Commun.*, 2011, **12**, 412–416.
37 J. W. Zheng, J. F. Zhou, H. Q. Lin, X. P. Duan, C. T. Williams and Y. Z. Yuan, *J. Phys. Chem. C*, 2015, **119**, 13758–13766.
38 E. K. Poels and D. S. Brands, *Appl. Catal., A*, 2000, **191**, 83–96.
39 Y. Wang, Y. L. Shen, Y. J. Zhao, J. Lv, S. P. Wang and X. B. Ma, *ACS Catal.*, 2015, **3**, 6200–6208.
40 X. P. Wang, M. Chen, X. K. Chen, R. H. Lin, H. J. Zhu, C. Q. Huang, W. S. Yang, Y. Tan, S. S. Wang, Z. N. Du and Y. J. Ding, *J. Catal.*, 2020, **383**, 254–263.